

## *Ab initio* calculation of optical properties with excitonic effects in wurtzite $\text{In}_x\text{Ga}_{1-x}\text{N}$ and $\text{In}_x\text{Al}_{1-x}\text{N}$ alloys

Luiz Cláudio de Carvalho,<sup>1,2,\*</sup> André Schleife,<sup>2,3</sup> Jürgen Furthmüller,<sup>1,2</sup> and Friedhelm Bechstedt<sup>1,2</sup>

<sup>1</sup>*Institut für Festkörpertheorie und -optik, Friedrich-Schiller-Universität, Max-Wien-Platz 1, 07743 Jena, Germany*

<sup>2</sup>*European Theoretical Spectroscopy Facility (ETSF)*

<sup>3</sup>*Condensed Matter and Materials Division, Lawrence Livermore National Laboratory, Livermore, California 94550, USA*

(Received 18 September 2012; revised manuscript received 3 March 2013; published 31 May 2013)

By combining modern many-body approaches with a cluster expansion scheme, frequency-dependent dielectric functions including excitonic and local-field effects are computed for wurtzitic group-III nitride alloys with varying composition  $x$ . The quasiparticle electronic structure required to construct the quasidelectron-quasihole pair Hamiltonian for each cluster is approximated using a LDA +  $U$  +  $\Delta$  approach. Two different cluster statistics are employed to perform configurational averages for the frequency-dependent complex dielectric functions. Comparing the resulting composition dependence of peak positions and intensities to experimental data allows conclusions regarding the distribution of the group-III cations in the alloys.

DOI: [10.1103/PhysRevB.87.195211](https://doi.org/10.1103/PhysRevB.87.195211)

PACS number(s): 78.20.Bh, 71.35.Cc, 78.20.Ci, 78.40.Fy

### I. INTRODUCTION

Group-III nitrides such as InN, GaN, and AlN have received considerable attention for high-power, high-frequency, and high-temperature electronic devices and for optoelectronic applications such as light-emitting and laser diodes.<sup>1</sup> Current advances in solid-state lighting are driven by tailoring their band gaps, for instance, in  $\text{In}_x\text{Ga}_{1-x}\text{N}$  and  $\text{In}_x\text{Al}_{1-x}\text{N}$  alloys. The binary nitrides crystallize in the wurtzite ( $wz$ ) structure, and the lowest direct optical transition across their fundamental band gaps of 0.7 eV (InN),<sup>2,3</sup> 3.5 eV (GaN),<sup>4</sup> and 6.2 eV (AlN)<sup>4</sup> is dipole allowed. Absorption and emission edges of their alloys, hence, cover the electromagnetic spectrum from the infrared to the ultraviolet.

However, since the growth of almost defect-free and homogeneous  $\text{In}_x\text{Ga}_{1-x}\text{N}$  and  $\text{In}_x\text{Al}_{1-x}\text{N}$  samples is a challenge for compositions  $x$  deviating significantly from the binary end components, alloys resulting from different growth experiments have been discussed controversially in the literature (see Ref. 5 and references therein). Clearly, a deeper understanding of the distribution of the cations in the alloy samples and the impact of the preparation conditions is needed.

Spectroscopic studies contribute to this understanding, and for technologically highly important alloys of hexagonal group-III nitrides such as  $\text{In}_x\text{Ga}_{1-x}\text{N}$ ,<sup>6–8</sup>  $\text{In}_x\text{Al}_{1-x}\text{N}$ ,<sup>9,10</sup> and  $\text{Al}_x\text{Ga}_{1-x}\text{N}$ ,<sup>11</sup> spectroscopic ellipsometry measurements of the optical properties exist, covering a wide spectral range. The variation of the line shape, peak positions, and intensities of the absorption spectra with composition  $x$  allows deep insight into the distribution of the group-III cations on their sublattice, the strength of composition fluctuations, and the appearance of clustering phenomena (see Refs. 5 and 12 and references therein). The interpretation of measured spectra, however, is not always easy and strongly benefits from the comparison to theoretical results that account for many-body effects,<sup>13–15</sup> as well as a reasonable description of alloying.<sup>5,16</sup>

Enormous progress has been made regarding the parameter-free description of optical properties including many-body effects based on calculations that fully take quasiparticle (QP) electronic structures and excitonic as well as local-field

effects (LFEs) into account (see Refs. 17 and 18, and references therein). For bulk semiconductors,<sup>19,20</sup> insulators,<sup>20,21</sup> surfaces,<sup>22</sup> nanostructures,<sup>23</sup> and molecules<sup>24</sup> it was shown that going from the independent-particle approximation to the independent-QP approximation, the optically excited noninteracting electron-hole pairs are replaced by noninteracting quasidelectron-quasihole pairs and, typically, the optical absorption spectra are significantly blueshifted; also,<sup>13</sup> the overall line shape is influenced because this shift is larger for peaks at higher energies.<sup>25</sup> Taking the screened attractive and unscreened repulsive interaction of quasidelectrons and quasiholes into account leads to a drastic redistribution of spectral strength from higher to lower photon energies combined with a redshift; these effects may render the picture of van Hove singularities questionable.<sup>14</sup> In addition, the absorption edge is significantly modified by the formation of bound excitonic states,<sup>26,27</sup> a phenomenon which can also appear in resonance at higher optical transitions.<sup>14,25</sup>

For bulk group-III nitrides in the  $wz$  or the zinc-blende structure,<sup>14,26,28–33</sup> the drastic influence of these many-body effects on line shape, peak positions, and peak intensities of optical absorption spectra has been shown previously. The resulting absorption coefficients and imaginary parts of the dielectric function (DF) are able to explain experimental findings. However, such sophisticated calculations of optical properties are still a challenge for alloys (more drastic approximations involving, for instance, empirical pseudopotentials were necessary in the past<sup>34</sup>) and have, so far, only been carried out for two oxide-based systems.<sup>16</sup>

In this paper, calculations of the optical spectra of  $wz$ - $\text{In}_x\text{Ga}_{1-x}\text{N}$  and  $wz$ - $\text{In}_x\text{Al}_{1-x}\text{N}$  alloys are presented and used to study the frequency-dependent DFs for different light polarizations and cluster statistics. In Sec. II the methodology is described and computational details are given. The success of the methods is demonstrated for bulk InN, GaN, and AlN in Sec. III. The influence of the alloy statistics and the composition on the main peaks of the DFs as well as the electronic dielectric constants are studied in detail in Sec. IV. Finally, in Sec. V a brief summary and conclusions are presented.

## II. THEORETICAL AND COMPUTATIONAL APPROACHES

### A. Modeling of alloys

The  $\text{In}_x\text{X}_{1-x}\text{N}$  ( $X = \text{Ga}, \text{Al}$ ) alloy may consist of  $N$  cations and  $N$  anions. Within a cluster expansion<sup>35–38</sup> it is divided into  $M$  clusters, each of which consists of  $2n$  atoms,  $n$  cations, and  $n$  anions (nitrogen). Consequently, it holds that  $N = nM$  for the total number of atoms on each of the sublattices. Due to symmetry (before ionic relaxation) the clusters can be grouped into  $J + 1$  different classes. Each class  $j = 0, \dots, J$  comprises  $g_j$  clusters of the same total energy and contributes with the cluster fraction  $x_j = M_j/M$  to the macroscopic alloy that is built by a set of  $\{M_j\}$  clusters. The number of In atoms in each class is denoted by  $n_j$ . Since the  $x_j$  describe the statistical weights, they are normalized according to  $\sum_{j=0}^J x_j = 1$  and  $\sum_{j=0}^J n_j x_j = xn$  for an alloy of the average composition  $x$ .

As done in previous works on wurtzitic systems,<sup>5,16,38,39</sup> we use 16-atom clusters (i.e.,  $n = 8$ ) that consist of four  $wz$  unit cells. A total number of  $\sum_{j=0}^J g_j = 2^n = 256$  possible clusters arises from assigning In or X atoms to all cation positions. Due to the symmetry of these, this number is divided into 22 classes and for each of these classes we use relaxed atomic geometries. Both the relaxations and their relation to Vegard's law are described in Ref. 5. For thermodynamic-equilibrium conditions at a given temperature and composition, the  $x_j$  can be determined within the generalized quasichemical approximation (GQCA).<sup>37,40</sup>

Here we study two limiting cases: (i) the strict-regular solution (SRS) model<sup>40</sup> for a random alloy (high-temperature limit of the GQCA) with cluster fractions

$$x_j^{\text{SRS}}(x) = g_j x^{n_j} (1-x)^{n-n_j} \quad (1)$$

and (ii) the microscopic decomposition model (MDM)

$$x_j^{\text{MDM}}(x) = \begin{cases} 1-x & \text{for } j=0 \\ x & \text{for } j=J \\ 0 & \text{otherwise} \end{cases}, \quad (2)$$

which describes the low-temperature limit of the GQCA with the strongest fluctuations of the composition on a microscopic length scale.<sup>16,38</sup>

The configurational average for a certain property of the alloy is related to the property  $P_j$  of a cluster material via the Connolly-Williams formula<sup>37,41</sup>

$$P(x) = \sum_{j=1}^J x_j(x) P_j. \quad (3)$$

The bowing of the composition dependence of an alloy property  $P$  can be described by<sup>5</sup>

$$P(x) = xP(\text{InN}) + (1-x)P(\text{XN}) - x(1-x)P_b(x), \quad (4)$$

$$P_b(x) = P_{b,0}/(1 + P_{b,1}x^2), \quad (5)$$

with a bowing parameter  $P_b(x)$  that can be composition-dependent itself, as indicated in Eq. (5). In Ref. 5 this has been discussed in detail for the fundamental band gaps of  $\text{In}_x\text{Ga}_{1-x}\text{N}$  and  $\text{In}_x\text{Al}_{1-x}\text{N}$ , and in the present work we investigate the frequency-dependent DF  $\epsilon_{\perp/\parallel}(\omega)$  for perpendicular

(ordinary) and parallel (extraordinary) light polarization (with respect to the  $c$  axis) as cluster properties. Hence, the optical spectra were computed for 22 individual cluster classes for each of the two alloys (leading to a total of 44 calculations).

### B. Quasiparticle electronic structure

It is well known that the Kohn-Sham eigenvalues of density functional theory<sup>42,43</sup> (DFT) cannot be identified with single-QP excitation energies  $\epsilon_{\nu\mathbf{k}}^{\text{QP}}$  (band  $\nu$ , Bloch wave vector  $\mathbf{k}$ ).<sup>15,44</sup> Recently, we demonstrated for AlN, InN, and GaN that a QP calculation based on Hedin's GW approximation starting from eigenvalues and eigenfunctions obtained using the nonlocal hybrid HSE06 exchange-correlation (XC) functional<sup>45–47</sup> yields interband energies in excellent agreement with measured results.<sup>5,14,48–50</sup> This so-called HSE +  $G_0W_0$  approach is, however, computationally too expensive for using it to calculate the starting electronic structure (QP eigenvalues, wave functions, Coulomb matrix elements) needed to set up the excitonic Hamiltonian. In addition, also the large number of  $\mathbf{k}$  points required to converge the optical spectra (e.g., in the vicinity of the absorption edge or in the frequency region where the imaginary part of the DF is rather constant) for all 22 cluster cells for  $\text{In}_x\text{Ga}_{1-x}\text{N}$  as well as  $\text{In}_x\text{Al}_{1-x}\text{N}$  makes it necessary to use a less expensive approach.

Therefore, throughout this work we rely on a procedure<sup>25,51</sup> where the HSE +  $G_0W_0$  QP eigenvalues and wave functions are mimicked by those of a DFT +  $U$  approach<sup>52,53</sup> and an additional scissors shift  $\Delta$ .<sup>16,18,27,33</sup> The parameter  $U$  describes a potential acting on the Ga  $3d$  and In  $4d$  shell and is determined such that the corresponding binding energies resemble the HSE +  $G_0W_0$  values. The scissors operator  $\Delta$  opens up the resulting band gaps to match the HSE +  $G_0W_0$  ones. In order for this DFT +  $U$  +  $\Delta$  scheme to work, the DFT +  $U$  gap has to be finite for all the cluster materials. When the AM05 XC functional is used,<sup>5</sup> this is, however, not the case for InN, even for unrealistically large values of  $U$ . For that reason we employ the local-density approximation (LDA), as parametrized by Perdew and Zunger,<sup>54</sup> to describe XC. Two values for  $U$ , 5.7 eV (Ga  $3d$ ) and 3.7 eV (In  $4d$ ), are used for all clusters because of the different localization of the Ga and In  $d$  states.

The LDA +  $U$  approach increases the LDA band gaps of the binary end components from 0.0 ( $wz$ -InN), 2.099 ( $wz$ -GaN), and 4.385 eV ( $wz$ -AlN) to 0.386, 2.474, and 4.385 eV, respectively. Since these gaps are smaller than HSE +  $G_0W_0$  results (0.638, 3.571, and 6.328 eV for the binary end components in 16-atom unit cells), the scissors operator  $\Delta$  is used to rigidly shift the conduction bands (CBs) up in energy. The shifts are derived for each cluster  $j$  so that the fundamental gaps are identical to the HSE +  $G_0W_0$  results published previously.<sup>5</sup> They vary nonlinearly with  $n_j$  from 0.252 eV (InN), to 1.097 eV (GaN), and 1.943 eV (AlN).

### C. Frequency-dependent dielectric function

In order to describe optical properties of the alloys, their frequency-dependent macroscopic DF  $\epsilon_{\perp/\parallel}(\omega)$  is studied as a central quantity. Solving the Bethe-Salpeter equation<sup>13,17,18</sup> for the optical polarization function<sup>55,56</sup> allows us to include

the attractive electron-hole interaction as well as LFEs. Neglecting the dynamics of the screening, the inhomogeneous Bethe-Salpeter equation can be replaced by a homogeneous eigenvalue problem for the singlet electron-hole pair Hamiltonian:<sup>13,18,33</sup>

$$\hat{H}(cv\mathbf{k},c'v'\mathbf{k}') = [\varepsilon_{c\mathbf{k}}^{\text{QP}} - \varepsilon_{v\mathbf{k}}^{\text{QP}}] \delta_{cc'} \delta_{vv'} \delta_{\mathbf{k}\mathbf{k}'} - W(cv\mathbf{k},c'v'\mathbf{k}') + 2\bar{v}(cv\mathbf{k},c'v'\mathbf{k}'). \quad (6)$$

The first summand in Eq. (6) describes the noninteracting quasielectron-quasihole pairs. The second term represents the screened Coulomb attraction  $W$  of pairs  $cv\mathbf{k}$  and  $c'v'\mathbf{k}'$ , while the third contribution describes their electron-hole exchange interaction and, hence, the LFEs. The eigenvalues  $E_\Lambda$  and eigenvectors  $A_\Lambda(cv\mathbf{k})$  of the pair Hamiltonian, Eq. (6), lead to the macroscopic DF via

$$\epsilon_{\perp/\parallel}(\omega) = 1 + \frac{8\pi e^2 \hbar^2}{Vm^2} \sum_{\Lambda} \left| \sum_{c,v,\mathbf{k}} \frac{\langle c\mathbf{k} | \mathbf{e}_{\perp/\parallel} \cdot \mathbf{p} | v\mathbf{k} \rangle}{\varepsilon_{c\mathbf{k}} - \varepsilon_{v\mathbf{k}}} A_{\Lambda}^*(cv\mathbf{k}) \right|^2 \times \sum_{\kappa=\pm,-} \frac{1}{E_{\Lambda} - \kappa \hbar(\omega + i\gamma)}, \quad (7)$$

with the momentum operator  $\mathbf{p}$  and the ordinary/extraordinary light polarization vector  $\mathbf{e}_{\perp/\parallel}$ .  $V$  denotes the volume of the crystal and  $\gamma$  describes the inverse electron-hole pair lifetime (chosen to be  $\gamma = 0.1$  eV).

Here, a model DF<sup>57,58</sup> describes the screening of the Coulomb potential in Eq. (6), which requires the static dielectric constant  $\epsilon_{\infty}$  for each cluster material. We use the static *electronic* dielectric constant (without any contribution of lattice polarization) calculated within random-phase approximation using the LDA +  $U$  scheme and averaged over the two independent components of the dielectric tensor. The number of CBs and  $\mathbf{k}$  points guarantees a convergence of the electronic dielectric constant on the order of 0.01.

A converged description of the absorption onset requires a very dense  $\mathbf{k}$ -point sampling<sup>14,27</sup> of the low-energy optical transitions, much higher than is necessary for calculations within the independent-QP approximation.<sup>59</sup> At the same time a large number of CBs is needed to describe the DF in a wide energy range. In order to fulfill both requirements, we employ different  $\mathbf{k}$ -point meshes for different photon energies: (i) A dense  $9 \times 9 \times 9$  Monkhorst-Pack (MP)<sup>60</sup>  $\mathbf{k}$ -point mesh is used to describe pair energies up to 3.5 eV (6.3 eV) in InGaN (InAlN), i.e., in the vicinity of the absorption edge. (ii) Photon energies up to 10 eV are described using a  $6 \times 6 \times 6$  MP mesh. (iii) All higher excitations up to 20 eV are computed using a less dense  $4 \times 4 \times 4$  MP  $\mathbf{k}$ -point mesh. Thereby, the number of bands (CBs) used for each  $\text{In}_j\text{X}_{8-j}\text{N}$  cluster material has been increased from 128 (96) in pure AlN to 288 (216) in pure InN according to the increasing number of  $d$  electrons in the cells. For InGaN 288 (216) bands (CBs) were used for all  $j$ .

This procedure still leads to large electron-hole pair Hamiltonians with ranks of up to 150,000; it is prohibitively expensive to directly diagonalize matrices that large. Instead, we compute the DFs for all the cluster materials using a time-propagation method<sup>13</sup> that relies only on matrix-vector multiplications and, hence, scales quadratically with the rank.

#### D. Computational framework

We use the Vienna ab initio simulation package (VASP)<sup>61</sup> to carry out the LDA +  $U$  calculations<sup>52,53</sup> that are necessary to set up<sup>18,62</sup> the excitonic Hamiltonians for each cluster material. The pseudopotentials have been generated within the projector-augmented-wave method<sup>63,64</sup> that allows us to compute valence  $s$  and  $p$  electronic states as well as In  $4d$  and Ga  $3d$  semicore states at all-electron quality. The wave functions are expanded into plane waves with a cutoff energy of 400 eV. Optical-transition matrix elements are computed within the longitudinal approximation.<sup>65</sup>

### III. DIELECTRIC FUNCTIONS FOR THE BINARY END COMPONENTS

In Fig. 1, the imaginary parts of the DF (including QP, excitonic, and LFEs) of  $wz$ -AlN,  $wz$ -GaN, and  $wz$ -InN, calculated for ordinary and extraordinary light polarization using the 16-atom cells, are compared to spectra measured by means of spectroscopic ellipsometry.<sup>66-71</sup> The oscillator strengths in Eq. (7) are proportional to the inverse of the squared interband energies, which leads to the  $\omega^{-2}$  decrease of the optical absorption for higher photon energies.<sup>72</sup> Apart from small deviations, the agreement between theoretical and experimental spectra with respect to the peak heights and positions is good. Particularly in the case of InN it is much better than reported for earlier calculations.<sup>30</sup> In addition, in the Supplemental Material<sup>73</sup> we compare the different spectra to the joint densities of states (JDOS) to highlight the importance of excitonic/LFEs as well as of optical dipole matrix elements (see Refs. S1 and S2).

In this work, the labels  $E_1, \dots, E_6$  are assigned to the peaks according to the energetical ordering of the peak structures. We use  $E_{A/B}$  ( $E_C$ ) to denote the peak that can be attributed to the lowest excitonic bound state that occurs for ordinary (extraordinary) light polarization. The corresponding transitions can be traced back to the uppermost (valence bands) VBs for the binary end components.<sup>5,50,74</sup> In earlier studies<sup>50,74</sup> we found that spin-orbit interaction introduces splittings of the uppermost VBs on the order of 10–25 meV, which is in good agreement with experimental results. Since that is much smaller than the energy scale that we use for studying the DFs in this work, we can safely neglect spin-orbit interaction here. Consequently, the selection rules are simplified and the labels  $A$  and  $B$  refer to transitions from the twofold degenerate  $\Gamma_5$  valence states into the CBs, and  $C$  is used for transitions from the  $\Gamma_1$ -type VB into the CBs.<sup>5,50,74</sup>

As indicated in Fig. 1, the majority of the measured peaks can be easily identified with peaks in the theoretical spectrum. The agreement is particularly good for the most pronounced absorption peak  $E_1$ , especially for AlN and GaN. Small differences between theory and experiment are found for the positions of  $E_2$  and  $E_3$  for GaN and are attributed to using the same scissors shift for all interband transitions and, hence, neglecting the energy dependence of QP corrections. In addition, especially for InN, the theoretical spectra show wiggling structures above the absorption onset, whereas the experimental spectra show an almost plateaulike region of the DF; simulating such a behavior as a sum of broadened

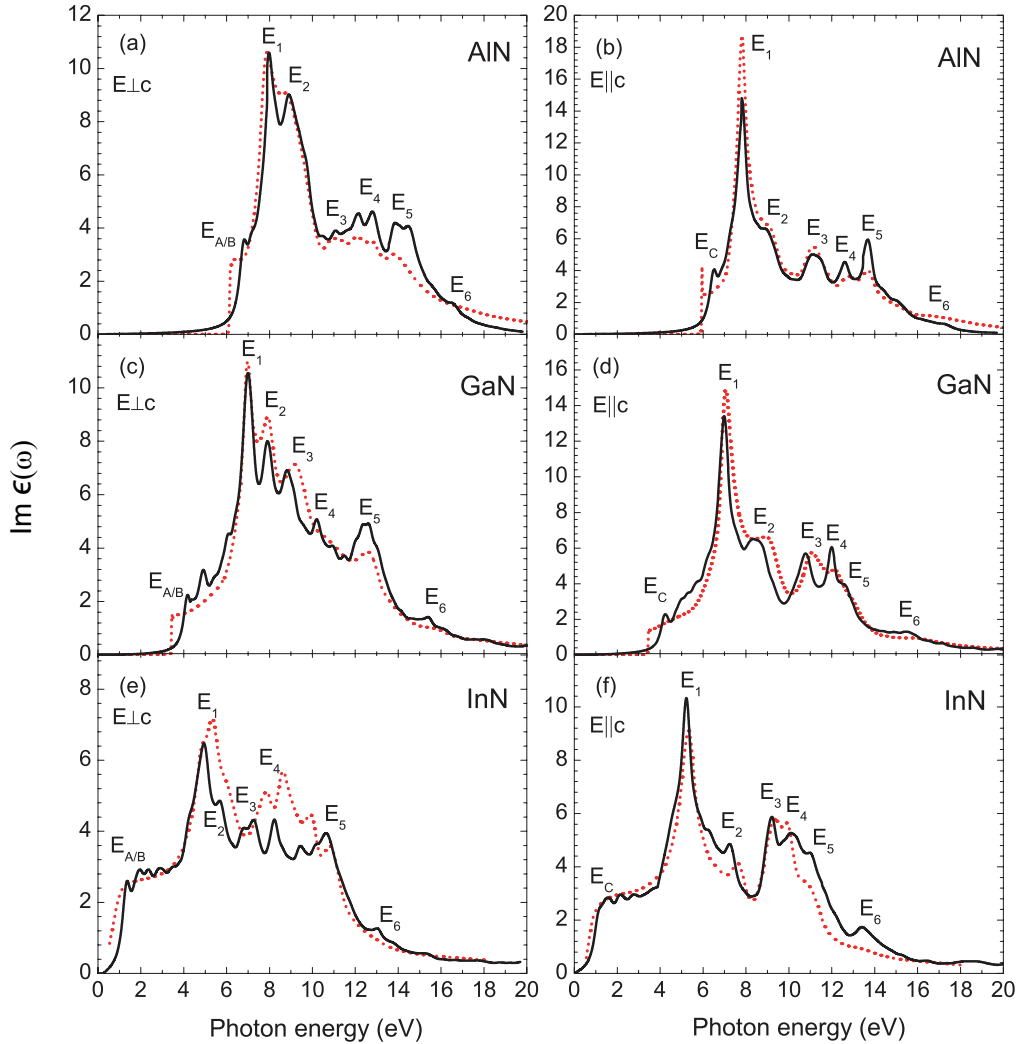


FIG. 1. (Color online) Imaginary part of the DF of  $wz$ -AlN (a, b),  $wz$ -GaN (c, d), and  $wz$ -InN (e, f) for ordinary (left panels) and extraordinary (right panels) light polarization. Black solid curves are calculated in this work using the 16-atom supercells and compared to experimental results (red dotted lines) for InN (Refs. 66 and 67), GaN (Refs. 68–70), and AlN (Refs. 68,69, and 71).

$\delta$  functions requires an even larger  $\mathbf{k}$ -point density, which is computationally too difficult. The small deviations of the spectra of  $wz$ -AlN compared to those from another recent study<sup>14</sup> can be traced back to the use of slightly different atomic geometries resulting from the different approximations to XC.

#### IV. RESULTS FOR THE ALLOYS

##### A. Absorption spectra

For ordinary and extraordinary light polarization the configurational averages of the DFs of  $\text{In}_x\text{Ga}_{1-x}\text{N}$  and  $\text{In}_x\text{Al}_{1-x}\text{N}$  are computed according to Eqs. (3) and (7) using the SRS and the MDM alloy statistics. All DFs and other results discussed below contain QP effects (calculated in the LDA +  $U$  +  $\Delta$  framework) as well as excitonic and LFEs computed for each individual cluster material. The imaginary parts of the DFs describe the optical absorption and are plotted in Figs. 2 and 3 for  $0 \leq x \leq 1$  over a wide range of photon energies. These figures allow the evolution of pronounced peak structures for varying In content  $x$  to be traced in the alloy. In the following, we discuss the influence of the alloy statistics.

In the case of the MDM [cf. Eq. (2)], the spectra in Figs. 2(c), 2(d), 3(c), and 3(d) are clearly related to the spectra of the binary end components: peak positions remain fixed at the values found for the binary systems (cf. Fig. 1) and the intensities are weighted by the probabilities  $1 - x$  (GaN or AlN) and  $x$  (InN). Also, the energy position of the absorption onset remains unchanged over a large composition range. These findings contradict the results of room-temperature spectroscopic-ellipsometry measurements<sup>7–10,69</sup> that show a pronounced variation of the optical gaps as well as of interband critical points with  $x$ . Therefore, we now focus on the results obtained within the SRS statistics, which is also supported by the detailed studies of the fundamental gaps of nitride alloys elsewhere.<sup>5</sup>

The random distribution of the clusters corresponding to the SRS model [cf. Eq. (1)] leads to variations of the peak positions and heights that are nonlinear with  $x$ . Figures 2(a), 2(b), 3(a), and 3(b) suggest that it is possible to follow a certain peak over a wide range of compositions with a rather continuous variation of the line shapes. However, this observation is misleading since different clusters and, hence, different optical transitions contribute to such an individual peak structure as the

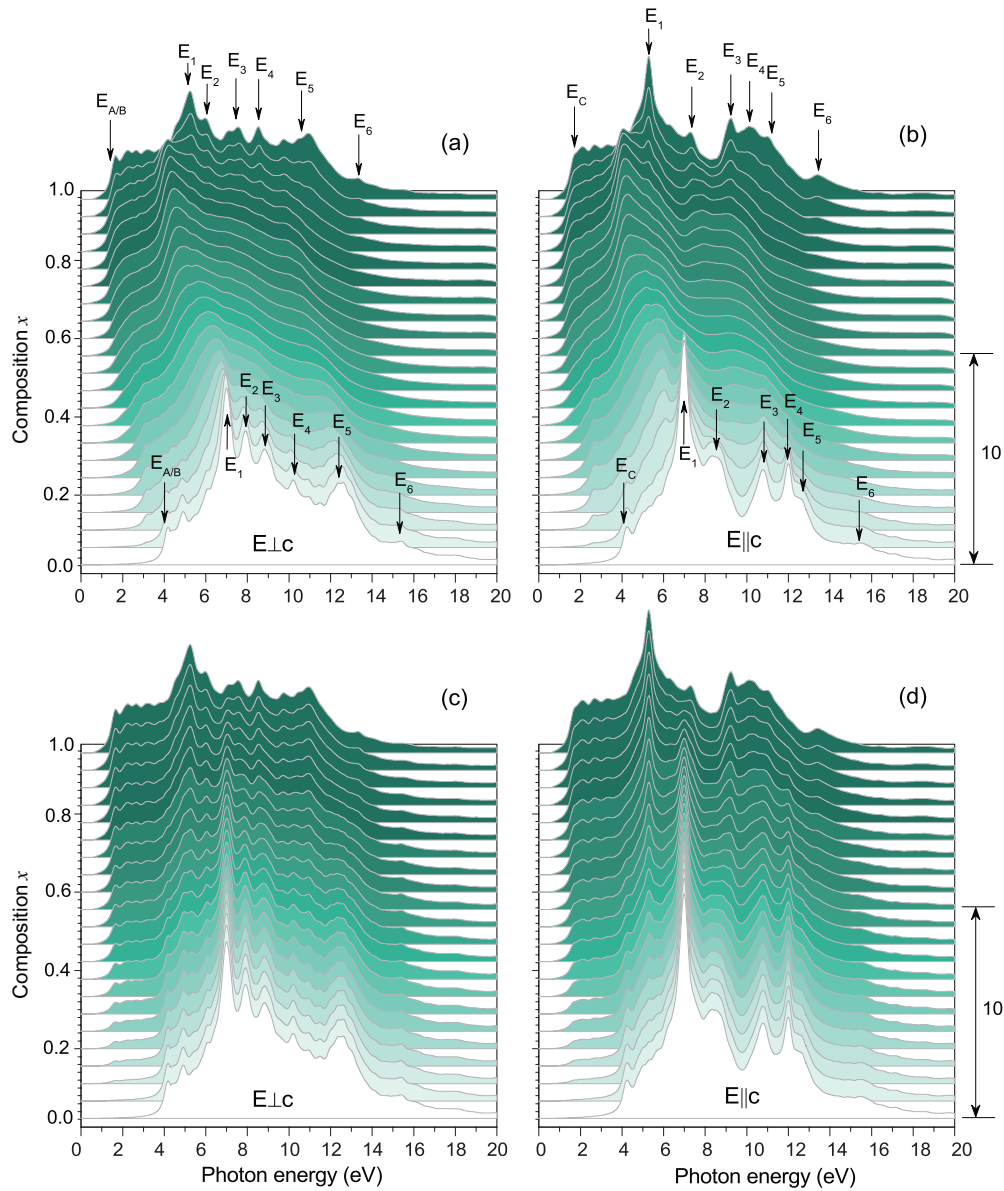


FIG. 2. (Color online) Imaginary part of the DF of  $wz$ - $\text{In}_x\text{Ga}_{1-x}\text{N}$  for ordinary (a, c) and extraordinary (b, d) light polarization as a function of the In composition  $x$ . The results for two different alloy statistics, SRS (a, b) and MDM (c, d), are shown. The peaks  $E_1, \dots, E_6$  (see text) and the absorption onsets ( $E_{A/B}$  and  $E_C$ ) are labeled. The bar indicates the scale for  $\text{Im } \epsilon_{\perp/\parallel}(\omega)$ .

composition  $x$  changes. Not only the intermixing of interband transitions by excitonic effects (that already occurs for the binary end components<sup>14</sup>) but also the alloying renders such an analysis impossible. Even though a band structure and a Brillouin zone (BZ) exists for each cluster material within the cluster expansion scheme, a symmetry analysis is not feasible due to the atomic relaxation of each cluster (which represents structural disorder) and the configurational average (which accounts for chemical disorder). For that reason it is not clear that electronic states of nearly the same symmetry contribute to a certain peak as the position and weight vary. We come back to this point in the next section.

Across the entire range of photon energies, the increasing influence of GaN [Figs. 2(a) and 2(b)] or AlN [Figs. 3(a) and 3(b)] becomes clear as  $x$  decreases from 1 to 0. The composition dependence is more pronounced for  $\text{In}_x\text{Al}_{1-x}\text{N}$

than for  $\text{In}_x\text{Ga}_{1-x}\text{N}$ , due to the larger fundamental band gap of AlN and the bigger range of weakly varying absorption between the onset and the first main peak in GaN. The variation of the main peak near 7.0 eV (GaN) or 7.5 eV (AlN) is weak and we will discuss the details of the higher interband transitions below.

While the influence of the different polarization directions is more striking near the end components, it is less pronounced for intermediate compositions  $x$ , as can be seen when comparing subfigures (a) and (b) of Figs. 2 and 3. One reason is that the structural disorder in the alloy modifies the dipole selection rules of higher-energy transitions. Hence, for compositions near the end components the  $wz$  symmetry is better preserved, leading to different dipole selection rules for the different light polarizations.<sup>50</sup> In addition, fewer clusters contribute for compositions close to the binary end components.

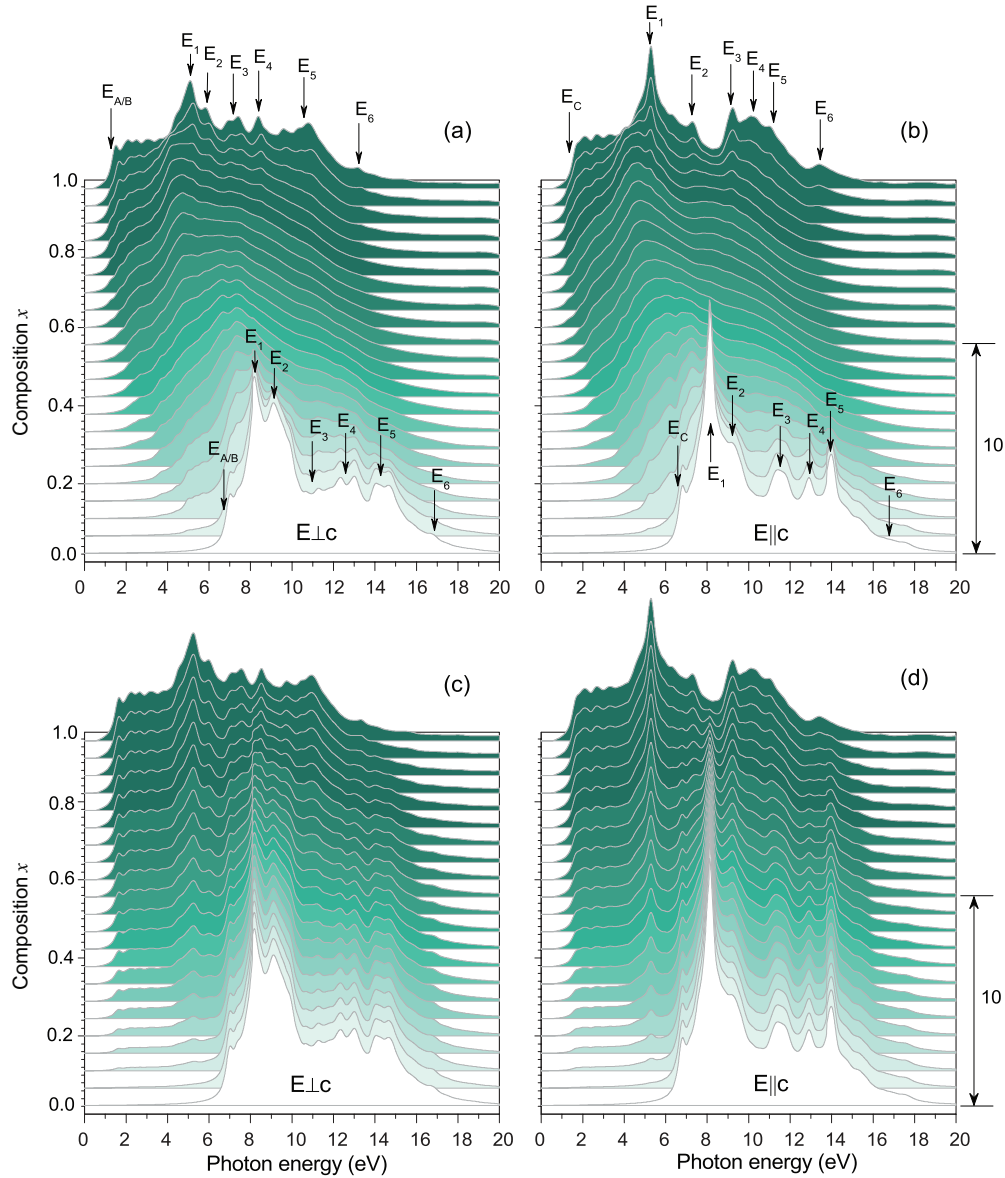


FIG. 3. (Color online) Imaginary part of the DF of  $wz\text{-In}_x\text{Al}_{1-x}\text{N}$  for ordinary (a, c) and extraordinary (b, d) light polarization as a function of the In composition  $x$ . The results for two different alloy statistics, SRS (a, b) and MDM (c, d), are shown. The peaks  $E_1, \dots, E_6$  (see text) and the absorption onsets ( $E_{A/B}$  and  $E_C$ ) are labeled. The bar indicates the scale for  $\text{Im } \epsilon_{\perp/\parallel}(\omega)$ .

### B. Interband critical points

The occurrence of pronounced peak structures in the imaginary parts of the DFs shown in Figs. 2 and 3 suggests an analysis of the composition dependence of the peak positions similar to that done when interpreting experimental spectra.<sup>7–10,69,75</sup> The underlying picture relies on the decomposition of Eq. (7) into a sum of oscillators  $j$  with energy  $E_j$ , oscillator strength  $C_j$ , and damping parameter  $\Gamma_j$ . Historically, this approach is driven by the idea that interband transitions govern the DF, and, due to the characteristic behavior of the JDOS near critical points, so-called van Hove singularities occur.<sup>76</sup> According to the nature of the critical points, this picture can be refined by taking excitonic effects into account.<sup>77</sup> In experimental studies of alloys [e.g.,  $\text{In}_x\text{Ga}_{1-x}\text{N}$  (Refs. 9 and 75) and In-rich  $\text{In}_x\text{Al}_{1-x}\text{N}$  (Refs. 7, 8, and 10)], the same procedure used for

crystals is applied and “critical points of the band structure” are resolved within certain composition ranges.

The composition dependence of several characteristic energies  $E_{A/B}$ ,  $E_C$ , and  $E_1, \dots, E_6$  has been derived from measured spectra based on this or a similar analysis.<sup>7–10,75</sup> In the following we adopt the picture of van Hove singularities, despite its limited validity due to the influence of optical transition matrix elements, excitonic effects, alloying, and contributions from  $\mathbf{k}$  points other than the high-symmetry ones.<sup>14</sup> For our analysis we relate the peaks  $E_1, \dots, E_6$  in the imaginary parts of the DFs of the binary end components (we follow the denotation in the experimental papers) to interband transitions at the  $\Gamma$ ,  $M$ ,  $K$ ,  $A$ ,  $L$ , and  $H$  high-symmetry points of the hexagonal BZ. Table I shows the energies of the corresponding transitions and their assignment to the different peaks. When comparing these transition energies to the peak

TABLE I. Characteristic interband energies (in electronvolts) related to the peak positions  $E_1, \dots, E_6$  in Figs. 3 and 4 for ordinary and extraordinary light polarization. The symmetry character and the position of the VB and CB extrema that determine the interband energy in the BZ are indicated. The interband energies follow from the LDA +  $U$  +  $\Delta$  approach.

Peak	Transition	Polarization	AlN	GaN	InN
$E_1$	$U_4 - U_1$	$\perp, \parallel$	–	6.57	4.63
	$M_4 - M_1$	$\perp, \parallel$	8.36	6.90	5.26
	$L_{1,3} - L_{1,3}$	$\parallel$	8.58	7.26	5.27
$E_2$	$M_2 - M_1$	$\perp$	9.80	8.12	6.08
	$K_3 - K_2$	$\parallel$	9.27	8.49	6.92
$E_3$	$H_3 - H_{1,2}$	$\parallel$	10.56	9.38	7.29
	$K_3 - K_3$	$\perp$	–	10.97	8.81
	$K_3 - K_2$	$\perp$	11.81	10.94	8.64
	$L_{1,3} - L_{1,3}$	$\perp$	–	10.59	9.10
$E_4$	$L_{1,3} - L_{1,3}$	$\perp$	12.55	10.57	8.43
	$L_{1,3} - L_{1,3}$	$\perp, \parallel$	12.93	10.59	9.10
	$L_{2,4} - L_{1,3}$	$\perp$	12.66	10.58	8.48
	$A_{5,6} - A_{1,6}$	$\parallel$	–	12.16	9.74
$E_5$	$A_{5,6} - A_{1,6}$	$\parallel$	–	12.16	10.27
	$H_3 - H_3$	$\parallel$	14.23	12.15	–
	$A_{1,3} - A_{5,6}$	$\parallel$	–	13.51	10.87
$E_6$	$A_{1,3} - A_{1,6}$	$\perp, \parallel$	16.75	15.41	13.11

positions in Figs. 2 and 3 one has to keep in mind that the interband energies are slightly higher than the peak energies because of the excitonic redshift. The results in Table I show that the identification of the peaks is possible, to some approximation, for the binary end components. For a more detailed study of the validity of the critical point picture in the presence of the excitonic effects, the reader is referred to Ref. 14.

However, in addition to these difficulties of unequivocally relating interband energies to a specific peak position, the composition dependence introduces a certain ambiguity for the alloys. For intermediate compositions the translational and point-group symmetries of the end components are not valid anymore and, in addition, configurational averages involving individual cluster materials  $\text{In}_{n_j}\text{X}_{8-n_j}\text{N}_8$  with composition-dependent lattice constants (i.e., varying extents of their BZs) are performed. We find that the assignment of peaks for compositions close to the end components is easier for  $\text{In}_x\text{Ga}_{1-x}\text{N}$  than for  $\text{In}_x\text{Al}_{1-x}\text{N}$  because the latter shows stronger internal strains and, hence, stronger atomic relaxations. Nevertheless, e.g., the  $E_1$  peak can be identified in the case of ordinary light polarization also for intermediate compositions  $x$ , where many classes of clusters contribute.

Difficulties with the identification are, however, obvious for the  $E_1$  peak from the SRS statistics. While it shifts relatively monotonically from GaN or AlN towards In-rich alloys, in both cases abrupt changes and even a peak splitting occur for compositions close to InN. Its position changes from 8.1 eV (7.2 eV) at  $x = 0$  to about 5.2 eV at  $x = 1$  in  $\text{In}_x\text{Al}_{1-x}\text{N}$  ( $\text{In}_x\text{Ga}_{1-x}\text{N}$ ) and bowing seems to be very strong. According to Table I, the main contributions are related to the lowest interband transitions on the  $L-M$  line in the BZ. While the identification seems to be obvious, for small  $x$  a second peak occurs for both  $\text{In}_x\text{Al}_{1-x}\text{N}$  and  $\text{In}_x\text{Ga}_{1-x}\text{N}$  that can be described by a strong nonlinear composition-dependent bowing.

TABLE II. Coefficients of the bowing parameter for higher interband transitions in the optical absorption spectra of Fig. 2 for  $\text{In}_x\text{Ga}_{1-x}\text{N}$ . Values for ordinary and extraordinary light polarization are given.

Transition	Ordinary		Extraordinary	
	$E_{b,0}$	$E_{b,1}$	$E_{b,0}$	$E_{b,1}$
1	4.43	–0.25	3.81	0.17
2	2.85	–0.44	3.98	–0.25
3	2.35	–0.34	3.51	–0.42
4	3.67	–0.43	3.83	–0.63
5	0.90	–0.54	5.16	–0.25
6	2.45	0.57	2.54	–0.43
$A/B, C$	2.07	1.16	3.82	1.47

For each of the individual  $\text{In}_{n_j}\text{Ga}_{8-n_j}\text{N}$  and  $\text{In}_{n_j}\text{Al}_{8-n_j}\text{N}$  cluster materials we extracted the positions of (the maxima of) the six peaks discussed above following their energetical order, i.e., they are not taken from Figs. 2 or 3. The results for all clusters are given in Fig. 4, along with the corresponding configurational averages of the energies within the SRS alloy statistics. For the reasons described above, the peaks cannot always be unequivocally assigned, but for  $\text{In}_x\text{Al}_{1-x}\text{N}$ , the peak identification for clusters with intermediate composition is particularly difficult. Hence, dotted lines are plotted in order to indicate the uncertainties, and in the following (as well as in Table II) we focus on  $\text{In}_x\text{Ga}_{1-x}\text{N}$  instead.

In Figs. 4(a) and 4(c) our theoretical results are compared to experimental values and we find that the agreement is very good for the  $E_{A/B}$  peaks both for  $\text{In}_x\text{Ga}_{1-x}\text{N}$  and  $\text{In}_x\text{Al}_{1-x}\text{N}$ . In the case of  $\text{In}_x\text{Ga}_{1-x}\text{N}$ , the higher-energy peaks determined from experiment practically coincide with our theoretical results; however, this is true only close to the binary end components [cf. Fig. 4(a)]. Especially the positions of the  $E_1, E_2$ , and  $E_4$  peaks seem to vary almost linearly with the composition and would, hence, be reasonably described within the MDM alloy statistics. For  $\text{In}_x\text{Al}_{1-x}\text{N}$  it can be seen in Fig. 4(c) that the agreement between experiment and theory is good, not only for the absorption onset, but also for  $E_1$  and  $E_2$ ; the deviations are larger in the case of  $E_3$ . However, the practical difficulties when assigning these peaks based on experimental or theoretical spectra should be listed as a possible reason for the observed disagreement, and also the dependence of the experimental (theoretical) results on the actual atomic geometries (cluster statistics).

The composition dependence of the peak maxima that is depicted in Fig. 4 exhibits a significant bowing which we describe by Eqs. (4) and (5). For the higher interband transitions in  $\text{In}_x\text{Ga}_{1-x}\text{N}$ , this leads to the parameters given in Table II. These values (except for the ones for  $E_5$ ) indicate that the bowing as described by  $E_{b,0}$  is very similar or only slightly larger than the one obtained for the fundamental gaps. However, there is a huge body of values for the bowing parameter of the fundamental gap (computed and measured) from the last 18 years. Summaries can be found in Refs. 5, 7, 12, and 75. The composition dependence of the bowing, quantified by  $E_{b,1}$ , is small. Only for the lowest absorption peaks  $E_{A/B}$  and  $E_C$  larger values are predicted.

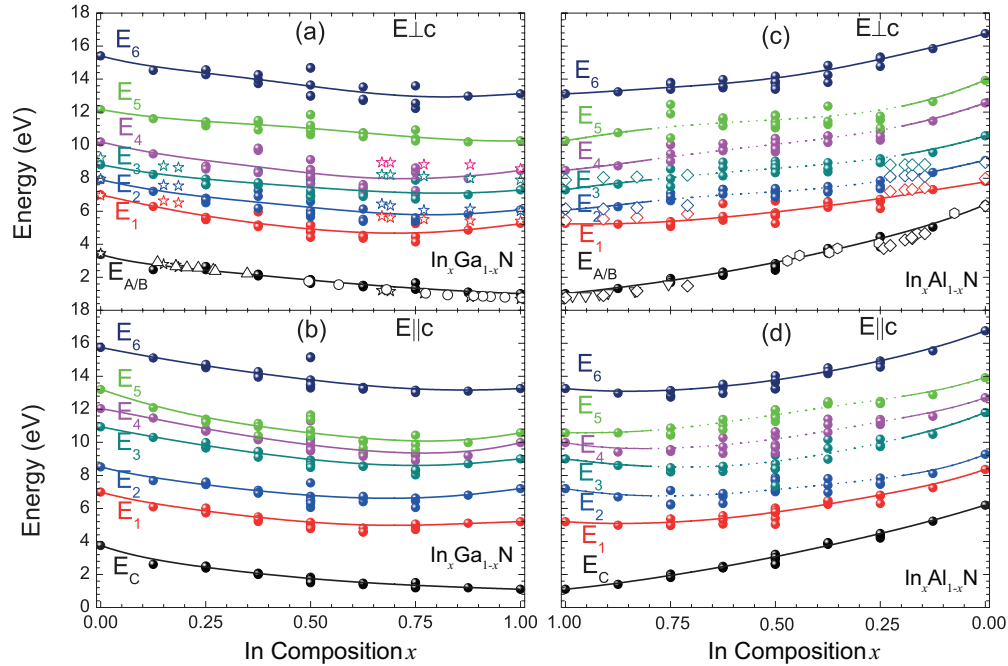


FIG. 4. (Color online) Configurational averages for the interband transition energies computed within the SRS model (solid lines) are shown for  $\text{In}_x\text{Ga}_{1-x}\text{N}$  (a, b) and  $\text{In}_x\text{Al}_{1-x}\text{N}$  (c, d). Results for ordinary (a, c) and extraordinary (b, d) light polarization are given. Large dots represent the corresponding energies for individual clusters. The dotted lines in (c, d) indicate the difficulties to identify the symmetry of interband transitions for  $\text{In}_x\text{Al}_{1-x}\text{N}$ . Experimental data is included as open symbols from Ref. 78 ( $\circ$ ), Ref. 79 ( $\triangle$ ), Refs. 7 and 75 ( $\star$ ), Ref. 10 ( $\diamond$ ), Ref. 80 ( $\nabla$ ), and Ref. 81 ( $\square$ ).

The order of magnitude of the bowing parameters agrees with results derived from measured spectra<sup>8,9</sup> but the theoretical values tend to be slightly larger (see, e.g., the  $b_i$  derived for  $E_1, \dots, E_6$  from measured data<sup>8,9</sup> and the values in Table II). We note that our theoretical results for the bowing parameters sensitively depend on the underlying cluster statistics. The apparent overestimation with respect to experiment may be attributed to using only the limiting case of the SRS cluster statistics to derive the data in Table II. At the same time such an explanation is somewhat in contrast to the findings for the fundamental absorption edge discussed in a previous paper,<sup>5</sup> where we have clearly stated that the composition dependence of the fundamental gap and the corresponding bowing (measured by absorption instead of photoluminescence) can be approximately explained using the SRS model. In this paper it is also clearly illustrated that fluctuations of observable quantities influence the bowing at a given average composition.

### C. Excitonic effects

Because of the small electronic dielectric constant of AlN (see Sec. IV D), the excitonic effects are expected to be strongest for  $\text{In}_x\text{Al}_{1-x}\text{N}$  alloys with small compositions  $x$ . This is confirmed by the values of the binding energies of the band-edge excitons that are largest (58 meV) for AlN (Ref. 82) and smaller for GaN (26 meV)<sup>83</sup> and InN (4 meV).<sup>27</sup> Hence, we focus on  $\text{In}_x\text{Al}_{1-x}\text{N}$  for the illustration of the excitonic effects in Fig. 5, where we plot the difference of the imaginary parts of the DFs with and without excitonic and LFEs. We note that the difference of the DFs with and without excitonic effects can

become negative in certain ranges of photon energies; however, here we focus on the energy region around the absorption edges of the individual cluster materials to illustrate bound excitonic states, Coulomb enhancement of the absorption edge, and redistribution of spectral strength from higher to lower photon energies. In this case, the difference is typically positive and, hence, we show only positive values in Fig. 5. We also distinguish between the two polarization directions as well as the MDM and the SRS model.

Due to the large screening in InN and GaN-rich alloys, bound-state-related peaks are only visible for AlN-rich alloys in Fig. 5. This becomes particularly clear from the difference spectra obtained within the MDM [cf. Figs. 5(b) and 5(d)], as they represent a linear interpolation of the difference spectra for the binary end components. For InN-rich alloys a redistribution of spectral strength as well as a Coulomb enhancement<sup>76</sup> is found; however, a peak related to excitonic bound states (due to transitions from the  $\Gamma_5^-$ - or  $\Gamma_1$ -type VB maximum) is only visible at the absorption onset of AlN-rich alloys. In the case of the SRS model, the difference spectra [see Figs. 5(a) and 5(c)] are completely different for intermediate compositions  $x$ . As discussed before, there is a continuous variation of the absorption edge modified by excitonic effects for compositions varying from  $x = 0$  to  $x = 1$ .

In addition, in Fig. 5, small arrows mark the QP gaps of individual clusters that significantly contribute to the configurational average at a certain composition  $x$ . This is important for the SRS model, because peaks that correspond to bound excitons of individual clusters may occur in the configurational average for the DF. In principle, these peaks represent resonant states in the DF since they appear near the

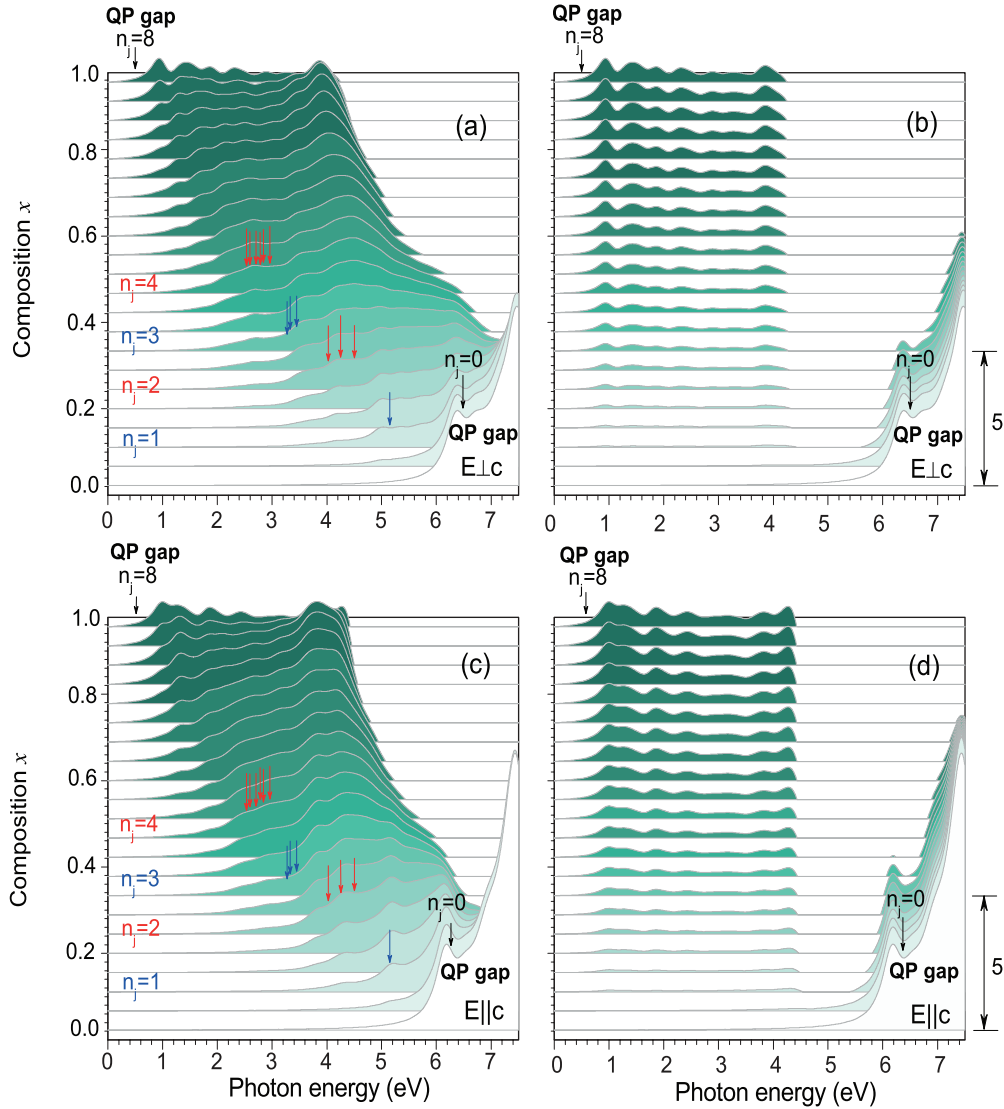


FIG. 5. (Color online) Difference in the imaginary parts of the DFs with and without excitonic/LFEs for  $\text{In}_x\text{Al}_{1-x}\text{N}$ . Results are shown for ordinary (a, b) and extraordinary (c, d) light polarization as well as the MDM (b, d) and the SRS model (a, c). The arrows indicate the QP gaps of the clusters that significantly contribute to the spectrum for a given average composition  $x$ . Only positive differences are shown (see text). The bar indicates the scale for the difference of the dielectric functions with and without excitonic effects.

energy position of the QP gap of the respective cluster, i.e., below the arrows in Figs. 5(a) and 5(c). In the alloy, clusters with a different composition already absorb light at these photon energies. Indeed, such a “bound” excitonic state below the QP edge occurs for the  $\text{In}_1\text{Al}_7\text{N}_8$  cluster material ( $n_j = 1$ ) for both polarization directions and also for  $n_j = 2$  such peaks are found. While their energy position does not significantly depend on the average composition  $x$  of the random alloy, the intensities are drastically reduced with increasing composition.

Since we calculate the spectrum of each individual cluster material using a periodic structure based on 16-atom supercells, local confinement effects on the electrons or holes are not taken into account. Quantum confinement related to strong composition fluctuations on a length scale of a few nanometers is not included in the present alloy description. The excitonic features computed within this work belong to a class of Wannier-Mott-like excitons.<sup>76</sup> Only those Wannier-Mott excitons with Bohr radii smaller than the extent of charac-

teristic composition fluctuations  $\Delta x$  are correctly described by our configurational averages. Using an effective-mass approximation<sup>76</sup> for the exciton binding, we estimate that the Bohr radii may vary in a range between about 1 nm (AlN-rich) and 10 nm (In-rich). When clustering and/or composition fluctuations<sup>5,30</sup> occur on a length scale that is smaller, our approach cannot correctly describe the excitonic effects.

#### D. Dielectric properties

The real part of the DF at vanishing frequency  $\text{Re } \epsilon(\omega = 0) \equiv \epsilon_\infty$  describes the tensor of the macroscopic electronic dielectric constants, exclusively reflecting electronic polarization (i.e., neglecting lattice polarization). In hexagonal crystals, it has two independent components  $\epsilon_{\infty,\perp}$  and  $\epsilon_{\infty,\parallel}$ . In contrast to many other theoretical works, we computed macroscopic electronic dielectric constants, including excitonic and local-field effects and not only values within the independent-particle or independent-QP approximation.<sup>59</sup> Using Eq. (5),

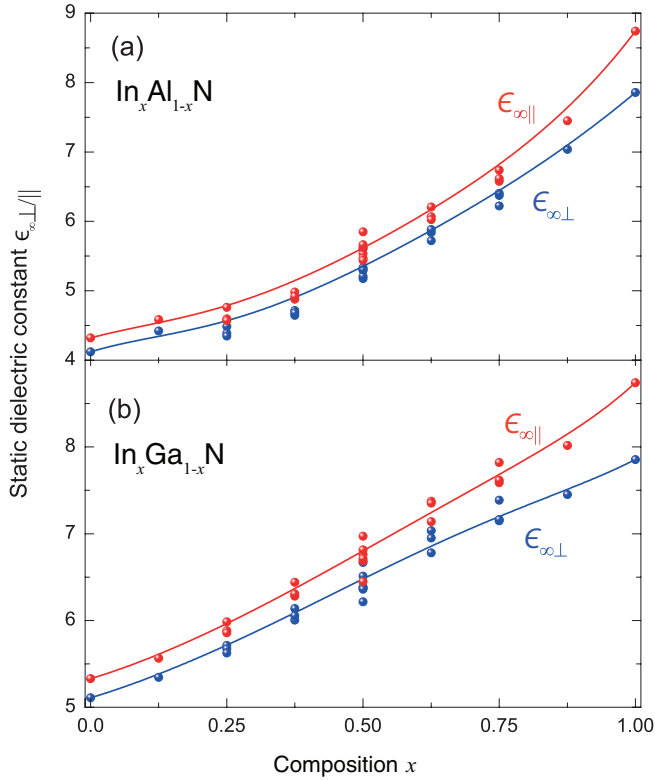


FIG. 6. (Color online) The independent components  $\epsilon_{\infty,\perp}$  (blue, ordinary polarization) and  $\epsilon_{\infty,\parallel}$  (red, extraordinary polarization) are plotted versus the average composition  $x$  for (a)  $\text{In}_x\text{Al}_{1-x}\text{N}$  and (b)  $\text{In}_x\text{Ga}_{1-x}\text{N}$  alloys described within the SRS model. The values for the individual cluster materials are indicated by dots.

which also accounts for many-body effects, we observe that the values for the macroscopic electronic dielectric constants  $\epsilon_{\infty,\perp}$  and  $\epsilon_{\infty,\parallel}$  within independent-particle approximation are by about 0.3...0.8 smaller.

Within our approach we obtain  $\epsilon_{\infty,\perp} = 4.12, 5.11,$  and  $7.86$  as well as  $\epsilon_{\infty,\parallel} = 4.32, 5.30,$  and  $8.74$  for AlN, GaN, and InN, respectively. The corresponding experimental values,<sup>84,85</sup>  $\epsilon_{\infty,\perp} = 4.14, 5.19,$  and  $7.83$  as well as  $\epsilon_{\infty,\parallel} = 4.28, 5.32,$  and  $8.03$ , are in excellent agreement. In the case of  $w_z\text{-InN}$  (extraordinary light polarization), the theoretical result slightly overestimates (by about 0.7) the electronic dielectric constant. This can be a consequence of using the LDA +  $U$  +  $\Delta$  method: the wave functions and, hence, the oscillator strengths might have a particularly large impact in the case of InN, which has the smallest energy gap. Also, experimental problems due to the difficulties of precisely measuring the electronic dielectric constant for light polarization parallel to the  $c$  axis in real samples cannot be excluded. Moreover, sample quality problems related to the real structure such as strain, free carriers, surfaces, and interfaces may occur.

The results for the configurational averages within the SRS model are plotted in Fig. 6 using the electronic dielectric constants calculated in this work. In order to illustrate the influence of the local geometries, also the electronic dielectric constants for the individual cluster materials are depicted in this figure. Figure 6 indicates some bowing, similar to that found for the fundamental energy gaps.<sup>5</sup> We describe the vari-

ation of the electronic dielectric constants with the composition using Eq. (4) along with a composition-independent bowing parameter  $\Delta\epsilon_{\infty,\perp/\parallel}$ . The bowing is most pronounced for the  $\text{In}_x\text{Al}_{1-x}\text{N}$  alloy, where  $\Delta\epsilon_{\infty,\perp} = 2.54$  and  $\Delta\epsilon_{\infty,\parallel} = 3.77$ . For  $\text{In}_x\text{Ga}_{1-x}\text{N}$  we obtain  $\Delta\epsilon_{\infty,\perp} = 0.09$  and  $\Delta\epsilon_{\infty,\parallel} = 1.05$ . The calculated composition dependence of  $\epsilon_{\infty,\perp}(x)$  for the AlN-rich alloy is close to variations found in experiment.<sup>10</sup>

## V. SUMMARY AND CONCLUSIONS

In this work we achieve the theoretical description of the optical properties of  $w_z\text{-In}_x\text{Ga}_{1-x}\text{N}$  and  $w_z\text{-In}_x\text{Al}_{1-x}\text{N}$  alloys based entirely on parameter-free calculations. Thereby, two approximations are important: (i) Each of the two alloys is modeled within a cluster expansion method using a total of 22 different clusters. Configurational averages are performed for the frequency-dependent DFs based on the DFs calculated for the individual cluster materials. The two limiting cases of a strict regular solution and a decomposition on a microscopic length scale are used for the cluster statistics. (ii) In order to derive the individual DFs, sophisticated many-body approaches are applied. Extremely dense  $\mathbf{k}$ -point meshes are used and the QP electronic structure is approximated within the LDA +  $U$  +  $\Delta$  scheme. The screened Coulomb attraction of quasielectrons and quasiholes as well as the unscreened electron-hole exchange interaction are taken into account to capture excitonic and LFEs that influence the entire spectra. Despite alloying, bound excitons remain visible below the absorption edge, especially for AlN-rich alloys.

We compare the composition dependence of the resulting absorption spectra to experimental findings for a wide photon-energy range, and we find indications that the cation distribution in the chemically disordered ternary compounds is better described by the strict regular solution model. However, we also note that in practice it is difficult to unequivocally assign peaks in the experimental or theoretical absorption spectrum across a large composition range because of strong variations of the atomic origin of these peaks. Close to the binary end components, important spectral features can approximately be explained by critical points in the band structure. However, for intermediate average compositions  $x$ , such a relation between electronic structure and optical absorption peaks becomes impossible, especially for  $\text{In}_x\text{Al}_{1-x}\text{N}$ . The bowing of higher interband transition energies is smaller than that found for the absorption edge.

Finally, also the macroscopic electronic dielectric constants calculated for the binary end components agree well with recent experimental findings. We find significant bowing for intermediate compositions in  $\text{In}_x\text{Al}_{1-x}\text{N}$ , while the bowing is much smaller for  $\text{In}_x\text{Ga}_{1-x}\text{N}$ .

## ACKNOWLEDGMENTS

We thank C. Rödl for interesting scientific discussions. The research presented here has received funding from the European Community's Seventh Framework Programme within the EU ITN RAINBOW (Grant No. 2008-2133278). Part of this work was performed under the auspices of the US Department of Energy at Lawrence Livermore National Laboratory under Contract No. DE-AC52-07A27344.

\*lccfísica@gmail.com

- <sup>1</sup>J. Wu, *J. Appl. Phys.* **106**, 011101 (2009).
- <sup>2</sup>V. Davydov, A. Klochikhin, R. Seisyan, V. Emtsev, S. Ivanov, F. Bechstedt, J. Furthmüller, H. Harima, A. Mudryi, A. Aderhold, O. Semchinova, and J. Graul, *Phys. Status Solidi B* **229**, R1 (2002).
- <sup>3</sup>J. Wu, W. Walukiewicz, K. M. Yu, J. W. Ager III, E. E. Haller, H. Lu, W. J. Schaff, Y. Saito, and Y. Nanishi, *Appl. Phys. Lett.* **80**, 3967 (2002).
- <sup>4</sup>I. Vurgaftman and J. R. Meyer, *J. Appl. Phys.* **94**, 3675 (2003).
- <sup>5</sup>L. C. de Carvalho, A. Schleife, J. Furthmüller, and F. Bechstedt, *Phys. Rev. B* **85**, 115121 (2012).
- <sup>6</sup>P. Schley, R. Goldhahn, A. T. Winzer, G. Gobsch, V. Cimalla, O. Ambacher, M. Rakel, C. Cobet, N. Esser, H. Lu, and W. J. Schaff, *Phys. Status Solidi B* **243**, 1572 (2006).
- <sup>7</sup>P. Schley, R. Goldhahn, A. T. Winzer, G. Gobsch, V. Cimalla, O. Ambacher, H. Lu, W. J. Schaff, M. Kurouchi, Y. Nanishi, M. Rakel, C. Cobet, and N. Esser, *Phys. Rev. B* **75**, 205204 (2007).
- <sup>8</sup>E. Sakalauskas, H. Behmenburg, P. Schley, G. Gobsch, C. Giesen, H. Kalisch, R. H. Jansen, M. Heuken, and R. Goldhahn, *Phys. Status Solidi A* **208**, 1517 (2011).
- <sup>9</sup>R. Goldhahn, P. Schley, A. T. Winzer, G. Gobsch, V. Cimalla, O. Ambacher, M. Rakel, C. Cobet, N. Esser, H. Lu, and W. J. Schaff, *Phys. Status Solidi A* **203**, 42 (2006).
- <sup>10</sup>E. Sakalauskas, H. Behmenburg, C. Hums, P. Schley, G. Rossbach, C. Giesen, M. Heuken, H. Kalisch, R. H. Jansen, J. Bläsing, A. Dadgar, A. Krost, and R. Goldhahn, *J. Phys. D: Appl. Phys.* **43**, 365102 (2010).
- <sup>11</sup>C. Buchheim, R. Goldhahn, M. Rakel, C. Cobet, N. Esser, U. Rossow, D. Fuhrmann, and A. Hangleiter, *Phys. Status Solidi B* **242**, 2610 (2005).
- <sup>12</sup>I. Gorczyca, S. P. Łepkowski, T. Suski, N. E. Christensen, and A. Svane, *Phys. Rev. B* **80**, 075202 (2009).
- <sup>13</sup>W. G. Schmidt, S. Glutsch, P. H. Hahn, and F. Bechstedt, *Phys. Rev. B* **67**, 085307 (2003).
- <sup>14</sup>A. Riefer, F. Fuchs, C. Rödl, A. Schleife, F. Bechstedt, and R. Goldhahn, *Phys. Rev. B* **84**, 075218 (2011).
- <sup>15</sup>G. Onida, L. Reining, and A. Rubio, *Rev. Mod. Phys.* **74**, 601 (2002).
- <sup>16</sup>A. Schleife, C. Rödl, J. Furthmüller, and F. Bechstedt, *New J. Phys.* **13**, 085012 (2011).
- <sup>17</sup>M. Rohlfing and S. G. Louie, *Phys. Rev. B* **62**, 4927 (2000).
- <sup>18</sup>C. Rödl, F. Fuchs, J. Furthmüller, and F. Bechstedt, *Phys. Rev. B* **77**, 184408 (2008).
- <sup>19</sup>S. Albrecht, L. Reining, R. Del Sole, and G. Onida, *Phys. Rev. Lett.* **80**, 4510 (1998).
- <sup>20</sup>L. X. Benedict, E. L. Shirley, and R. B. Bohn, *Phys. Rev. Lett.* **80**, 4514 (1998).
- <sup>21</sup>M. Rohlfing and S. G. Louie, *Phys. Rev. Lett.* **81**, 2312 (1998).
- <sup>22</sup>P. H. Hahn, W. G. Schmidt, and F. Bechstedt, *Phys. Rev. Lett.* **88**, 016402 (2001).
- <sup>23</sup>M. Bruno, M. Palummo, A. Marini, R. DelSole, and S. Ossicini, *Phys. Rev. Lett.* **98**, 036807 (2007).
- <sup>24</sup>P. H. Hahn, W. G. Schmidt, and F. Bechstedt, *Phys. Rev. B* **72**, 245425 (2005).
- <sup>25</sup>A. Schleife, C. Rödl, F. Fuchs, J. Furthmüller, and F. Bechstedt, *Phys. Rev. B* **80**, 035112 (2009).
- <sup>26</sup>R. Laskowski, N. E. Christensen, G. Santi, and C. Ambrosch-Draxl, *Phys. Rev. B* **72**, 035204 (2005).
- <sup>27</sup>F. Fuchs, C. Rödl, A. Schleife, and F. Bechstedt, *Phys. Rev. B* **78**, 085103 (2008).
- <sup>28</sup>L. X. Benedict and E. L. Shirley, *Phys. Rev. B* **59**, 5441 (1999).
- <sup>29</sup>L. Benedict, T. Wethkamp, K. Wilmers, C. Cobet, N. Esser, E. Shirley, W. Richter, and M. Cardona, *Solid State Commun.* **112**, 129 (1999).
- <sup>30</sup>J. Furthmüller, P. H. Hahn, F. Fuchs, and F. Bechstedt, *Phys. Rev. B* **72**, 205106 (2005).
- <sup>31</sup>F. Bechstedt, K. Seino, P. H. Hahn, and W. G. Schmidt, *Phys. Rev. B* **72**, 245114 (2005).
- <sup>32</sup>P. H. Hahn, K. Seino, W. G. Schmidt, J. Furthmüller, and F. Bechstedt, *Phys. Status Solidi B* **242**, 2720 (2005).
- <sup>33</sup>F. Bechstedt, F. Fuchs, and J. Furthmüller, *Phys. Status Solidi A* **207**, 1041 (2010).
- <sup>34</sup>A. Hafaiedh and N. Bouarissa, *Mater. Chem. Phys.* **1**, 122 (2009).
- <sup>35</sup>A. Sher, M. van Schilfgaarde, A.-B. Chen, and W. Chen, *Phys. Rev. B* **36**, 4279 (1987).
- <sup>36</sup>S.-H. Wei, L. G. Ferreira, and A. Zunger, *Phys. Rev. B* **41**, 8240 (1990).
- <sup>37</sup>L. K. Teles, J. Furthmüller, L. M. R. Scolfaro, J. R. Leite, and F. Bechstedt, *Phys. Rev. B* **62**, 2475 (2000).
- <sup>38</sup>A. Schleife, M. Eisenacher, C. Rödl, F. Fuchs, J. Furthmüller, and F. Bechstedt, *Phys. Rev. B* **81**, 245210 (2010).
- <sup>39</sup>C. Caetano, L. K. Teles, M. Marques, A. Dal Pino, and L. G. Ferreira, *Phys. Rev. B* **74**, 045215 (2006).
- <sup>40</sup>A.-B. Chen and A. Sher, *Semiconductor Alloys* (Plenum, New York, 1995).
- <sup>41</sup>J. W. D. Connolly and A. R. Williams, *Phys. Rev. B* **27**, 5169 (1983).
- <sup>42</sup>P. Hohenberg and W. Kohn, *Phys. Rev.* **136**, B864 (1964).
- <sup>43</sup>W. Kohn and L. J. Sham, *Phys. Rev.* **140**, A1133 (1965).
- <sup>44</sup>M. S. Hybertsen and S. G. Louie, *Phys. Rev. B* **34**, 5390 (1986).
- <sup>45</sup>J. Heyd, G. E. Scuseria, and M. Ernzerhof, *J. Chem. Phys.* **124**, 219906 (2006).
- <sup>46</sup>J. Paier, M. Marsman, K. Hummer, G. Kresse, I. C. Gerber, and J. G. Ángyán, *J. Chem. Phys.* **124**, 154709 (2006).
- <sup>47</sup>J. Paier, M. Marsman, K. Hummer, G. Kresse, I. C. Gerber, and J. G. Ángyán, *J. Chem. Phys.* **125**, 249901 (2006).
- <sup>48</sup>F. Fuchs, J. Furthmüller, F. Bechstedt, M. Shishkin, and G. Kresse, *Phys. Rev. B* **76**, 115109 (2007).
- <sup>49</sup>F. Bechstedt, F. Fuchs, and G. Kresse, *Phys. Status Solidi B* **246**, 1877 (2009).
- <sup>50</sup>L. C. de Carvalho, A. Schleife, and F. Bechstedt, *Phys. Rev. B* **84**, 195105 (2011).
- <sup>51</sup>A. Schleife, C. Rödl, F. Fuchs, J. Furthmüller, F. Bechstedt, P. H. Jefferson, T. D. Veal, C. F. McConville, L. F. J. Piper, A. DeMasi, K. E. Smith, H. Lösch, R. Goldhahn, C. Cobet, J. Zúñiga-Pérez, and V. Muñoz-Sanjosé, *J. Korean Phys. Soc.* **53**, 2811 (2008).
- <sup>52</sup>S. L. Dudarev, G. A. Botton, S. Y. Savrasov, C. J. Humphreys, and A. P. Sutton, *Phys. Rev. B* **57**, 1505 (1998).
- <sup>53</sup>V. I. Anisimov, J. Zaanen, and O. K. Andersen, *Phys. Rev. B* **44**, 943 (1991).
- <sup>54</sup>J. P. Perdew and A. Zunger, *Phys. Rev. B* **23**, 5048 (1981).
- <sup>55</sup>W. Hanke and L. J. Sham, *Phys. Rev. Lett.* **43**, 387 (1979).
- <sup>56</sup>G. Strinati, *Riv. Nuovo Cimento* **11**, 1 (1988).
- <sup>57</sup>F. Bechstedt, R. Del Sole, G. Cappellini, and L. Reining, *Solid State Commun.* **84**, 765 (1992).

- <sup>58</sup>G. Cappellini, R. Del Sole, L. Reining, and F. Bechstedt, *Phys. Rev. B* **47**, 9892 (1993).
- <sup>59</sup>B. Adolph, V. I. Gavrilenko, K. Tenelsen, F. Bechstedt, and R. Del Sole, *Phys. Rev. B* **53**, 9797 (1996).
- <sup>60</sup>H. J. Monkhorst and J. D. Pack, *Phys. Rev. B* **13**, 5188 (1976).
- <sup>61</sup>G. Kresse and J. Furthmüller, *Phys. Rev. B* **54**, 11169 (1996).
- <sup>62</sup>C. Rödl, F. Fuchs, J. Furthmüller, and F. Bechstedt, *Phys. Rev. B* **79**, 235114 (2009).
- <sup>63</sup>P. E. Blöchl, *Phys. Rev. B* **50**, 17953 (1994).
- <sup>64</sup>G. Kresse and D. Joubert, *Phys. Rev. B* **59**, 1758 (1999).
- <sup>65</sup>M. Gajdoš, K. Hummer, G. Kresse, J. Furthmüller, and F. Bechstedt, *Phys. Rev. B* **73**, 045112 (2006).
- <sup>66</sup>P. Schley, J. Räthel, E. Sakalauskas, G. Gobsch, M. Wieneke, J. Bläsing, A. Krost, G. Koble Müller, J. S. Speck, and R. Goldhahn, *Phys. Status Solidi A* **207**, 1062 (2010).
- <sup>67</sup>R. Goldhahn, A. Winzer, V. Cimalla, O. Ambacher, C. Cobet, W. Richter, N. Esser, J. Furthmüller, F. Bechstedt, H. Lu, and W. J. Schaff, *Superlattices Microstruct.* **36**, 591 (2004).
- <sup>68</sup>M. Röppischer, Ph.D. thesis, TU-Berlin, 2011.
- <sup>69</sup>M. Feneberg, M. Röppischer, C. Cobet, N. Esser, B. Nenshl, K. Thonke, M. Bickermann, M. F. Romero, and R. Goldhahn (unpublished).
- <sup>70</sup>C. Cobet, R. Goldhahn, W. Richter, and N. Esser, *Phys. Status Solidi B* **246**, 1440 (2009).
- <sup>71</sup>G. Rossbach, M. Röppischer, P. Schley, G. Gobsch, C. Werner, C. Cobet, N. Esser, A. Dadgar, M. Wieneke, A. Krost, and R. Goldhahn, *Phys. Status Solidi B* **247**, 1679 (2010).
- <sup>72</sup>G. Grosso and G. Pastori Parravicini, *Solid State Physics* (Academic Press, Amsterdam, 2000).
- <sup>73</sup>See Supplemental Material at <http://link.aps.org/supplemental/10.1103/PhysRevB.87.195211> for comparing the different spectra to the joint densities of states.
- <sup>74</sup>L. C. de Carvalho, A. Schleife, F. Fuchs, and F. Bechstedt, *Appl. Phys. Lett.* **97**, 232101 (2010).
- <sup>75</sup>E. Sakalauskas, O. Tuna, A. Kraus, H. Bremers, U. Rossow, C. Giesen, M. Heuken, A. Hangleiter, G. Gobsch, and R. Goldhahn, *Phys. Status Solidi B* **249**, 485 (2012).
- <sup>76</sup>P. Yu and M. Cardona, *Fundamentals of Semiconductors* (Springer-Verlag, Berlin, 1999).
- <sup>77</sup>D. E. Aspnes, *Phys. Rev. Lett.* **28**, 168 (1972).
- <sup>78</sup>J. Wu, W. Walukiewicz, W. Shan, K. M. Yu, J. W. Ager, E. E. Haller, H. Lu, and W. J. Schaff, *Phys. Rev. B* **66**, 201403 (2002).
- <sup>79</sup>K. P. O'Donnell, I. Fernandez-Torrente, P. R. Edwards, and R. W. Martin, *J. Cryst. Growth* **269**, 100 (2004).
- <sup>80</sup>W. Walukiewicz, S. X. Li, J. Wu, K. M. Yu, J. W. Ager, E. E. Haller, H. Lu, and W. J. Schaff, *J. Cryst. Growth* **269**, 119 (2004).
- <sup>81</sup>T. Onuma, S. Chichibu, Y. Uchinuma, T. Sota, S. Yamaguchi, S. Kamiyama, H. Amano, and I. Akasaki, *J. Appl. Phys.* **94**, 2449 (2003).
- <sup>82</sup>G. Rossbach, M. Feneberg, M. Röppischer, C. Werner, N. Esser, C. Cobet, T. Meisch, K. Thonke, A. Dadgar, J. Blasing, A. Krost, and R. Goldhahn, *Phys. Rev. B* **83**, 195202 (2011).
- <sup>83</sup>A. V. Rodina, M. Dietrich, A. Göldner, L. Eckey, A. Hoffmann, A. L. Efros, M. Rosen, and B. K. Meyer, *Phys. Rev. B* **64**, 115204 (2001).
- <sup>84</sup>P. Schley, R. Goldhahn, G. Gobsch, M. Feneberg, K. Thonke, X. Wang, and A. Yoshikawa, *Phys. Status Solidi B* **246**, 1177 (2009).
- <sup>85</sup>S. Shokhovets, R. Goldhahn, G. Gobsch, S. Piekh, R. Lantier, A. Rizzi, V. Lebedev, and W. Richter, *J. Appl. Phys.* **94**, 307 (2003).